Urban Climate 48 (2023) 101429

Contents lists available at ScienceDirect

Urban Climate

journal homepage: www.elsevier.com/locate/uclim

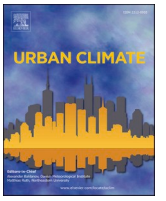

Contrasting effects of lake breeze and urbanization on heat stress in Chicago metropolitan area

Jiali Wang [a,*], Yun Qian [b], William Pringle [a], T.C. Chakraborty [b], Robert Hetland [b], Zhao Yang [b], Pengfei Xue [a,c]

[a] Environmental Science Division, Argonne National Laboratory, 9700 Cass Avenue, Lemont, IL 60439, USA
[b] Pacific Northwest National Laboratory, P.O. Box 999, Richland, WA 99352, USA
[c] Department of Civil, Environmental and Geospatial Engineering, Michigan Technological University, Houghton, MI 49931, USA

ARTICLE INFO

Keywords:
Lake breeze
Urbanization
Heat stress

ABSTRACT

This study used the latest Weather Research and Forecasting (WRF) model coupled with multi-layer urban canopy models to investigate contrasting effects from urbanization and lake breeze on summer heat stress over the Chicago metropolitan area (CMA). Comparisons between the model and in situ observations show that this coupled modeling system better captures urban locations' diurnal pattern of surface air temperature, skin temperature and relative humidity, with root mean square error reduced from 1.58 to 1.80 °C to 1.14–1.31 °C, 3.11–3.55 °C to 1.81–2.21 °C, and 10.73–11.35% to 7.84–8.60%, respectively, compared to WRF without coupling the urban canopy models. Two sensitivity experiments were conducted to isolate the influence of lake breeze and urbanization: one replaced the urban land use with cropland over the CMA, and the other filled all of Lake Michigan with cropland. Three different heat stress indices were computed to assess the uncertainties of heat stress response to changes in air temperature, relative humidity, and wind conditions. Results show that, when the lake has the largest cooling effect on air temperature, it also increases the relative humidity the most, and vice versa for urban warming and drying effects. Urbanization intensifies heat stress at night, and extends the heat caution period by up to 4 h over inland urban grids; the lake breeze relieves heat stress during afternoon (when the heat stress is the worst), and shortens the heat caution period by 1–3 h over inland urban grids and 3–4 h over coastal urban grids. The intensification of heat stress over the CMA due to urbanization is more than four times greater than the reduction from the lake breeze in the late afternoon and evening.

1. Introduction

The frequency of heatwaves is likely to increase over most land areas on Earth in the 21st century (Solomon et al., 2007). As a result, multiple adverse outcomes are expected, including increased heat stress, heat strokes, and heat-related mortality. In the United States, heatwaves are expected to become more intense, more frequent, and longer lasting (Meehl and Tebaldi, 2004; Ebi and Meehl, 2007; Smith et al., 2013; Zobel et al., 2017). The human physiological response to heat depends on both air temperature and relative humidity; their combined impact is commonly described by heat indices (HIs), also known as "feels like" temperatures. Dahl et al. (2019)

* Corresponding author.
E-mail address: jialiwang@anl.gov (J. Wang).

https://doi.org/10.1016/j.uclim.2023.101429
Received 16 July 2022; Received in revised form 28 October 2022; Accepted 19 January 2023
Available online 28 January 2023

projected that the annual numbers of days with HIs (using the same index we use; see Sect. 2.2.2) above 37.8 °C (100 °F) will doubled, and above 40.6 °C (105 °F) will triple, by the mid-21st century (2036–2065), compared to a 1971–2000 baseline. Cities are more vulnerable to extreme heat than rural areas because of pre-existing urban heat island (UHI) effects generated by air conditioning units, motor vehicles, generators, buildings and dark surfaces, radiative and thermodynamic modifications of the land surface, and other heat sources (Oke, 1982; Grimmond, 2007; Qian et al., 2022). Urban areas currently accommodate nearly half of the global population, and this fraction is projected to increase to 0.68 by 2050 (Grimm et al., 2008). This combination of urban population growth and the UHI makes heat stress in cities a great threat to human health and well-being (Anderson and Bell, 2011).

The Chicago metropolitan area (CMA) is a high-density residential area along the shore of Lake Michigan. It covers 12 counties in Illinois, 2 in Wisconsin, and 2 in Indiana. According to U.S. Census Bureau data, 48.4% of the Illinois population lives in Cook County and DuPage County (~6.2 million people), where the city of Chicago and most of its suburbs are located. Geographically, Chicago is located on a relatively flat terrain on the southwestern side of Lake Michigan. During the summer, the land areas are hotter than Lake Michigan, especially in the afternoon. This temperature difference creates a high-pressure ridge over the lake and low pressure over the land, causing hot air to rise over the CMA. This vertical transport results in a lake breeze (Laird et al., 2001): cooler near-surface air flows from the lake to the land. The effects of the lake breeze on the near-surface atmosphere over the CMA have been investigated via measurements and numerical modeling in several previous studies (Keeler and Kristovich, 2012; Meir et al., 2013; Conry et al., 2014, 2015). These studies found that the lake breeze from Lake Michigan can penetrate 15–30 km inland, moving cool and humid air from Lake Michigan into the cities on the western side of the lake, providing cool temperatures to relieve heat stress in the CMA during intense heatwaves (Kunkel et al., 1996). The most significant impacts occur near the lakeshore (Atkinson, 2003; Laird et al., 2001). On the other hand, lake breeze may be accelerated toward the city center by the enlarged temperature gradient between lake and urban area, and the UHI center may be displaced due to the lake breeze propagation (Ackerman, 1985; Gedzelman et al., 2003; Chemel and Sokhi, 2012). Based on radar and surface observations, Keeler and Kristovich (2012) found that a high nighttime UHI is well correlated with a low speed of lake-breeze frontal movement (during the daytime) throughout Chicago's southwest suburbs. Using Weather Research and Forecasting (WRF) coupled with various urban models, Sharma et al. (2017) found that when urban grids are replaced by cropland, the lake breeze is not as strong; however, it can still penetrate inland as much as when the urban area is in place. Similar to lake breeze, the temperature differences between urban (warmer) and rural (cooler) areas can also induce circulation – converging toward the city near the ground surface, uplifting over the city center, diverging at altitude, and descending outside the city limits (Hidalgo et al., 2010). Therefore, coastal cities are influenced by both of these thermally driven circulations (lake-to-urban flow, and rural-to-urban flow) and their interactions (Fig. 1). Additional studies around the world have shown similar strong interactions between rural, urban and coastal regions (Ohashi and Kida, 2002; Hu and Xue, 2016; Ribeiro et al., 2018; Umezaki et al., 2020).

Despite the worldwide studies that have been conducted, questions persist about the relative effects of the lake and urbanization on heat stress in the CMA. First, previous studies mainly focused on air temperature and omitted relative humidity, which is equally important because (1) it also influences the severity of heat hazards related to human health; and (2) urbanization and lake breeze can influence both air temperature and humidity. Second, the previous studies either used simplified models or in situ observations, which limits the possibility of understanding the interactions between each of the components (e.g., water, urban, and rural effect). Those studies that used comprehensive numerical models primarily focused on individual events over a particular urban area, making it challenging to transfer the knowledge learned to other events or other coastal urban areas. The current study uses WRF with a configuration calibrated for this lake–land interface coupled with an updated multilayer building environment parameterization (BEP) model and a multilayer building energy model (BEM) to study the competing effects of urbanization and lake breeze on heat stress over the CMA. We choose the CMA as a testbed because (1) it has a history of heatwave events (Kunkel et al., 1996; Karl and Knight, 1997; Ebi and Meehl, 2007); (2) the terrain is flat, which simplifies atmospheric circulation in the region; (3) there are no other nearby major metropolitan regions: from one direction Chicago borders a major water body, and in the other direction there is a fairly homogenous agricultural landscape, promoting a clear delineation of the singular effect of each of these components. Instead of examining

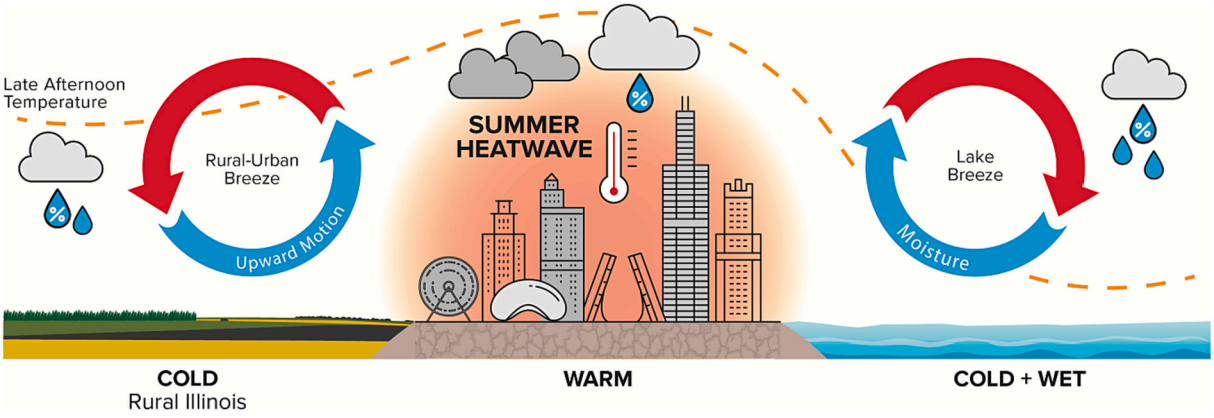

Fig. 1. Schematic picture of the coastal urban system (Chicago in particular) and local circulations caused by temperature difference across different land cover types during late afternoon.

individual events, this study assesses isolated effects of and interactions between urbanization and lake breeze over an entire summer at diurnal scale. While previous studies mostly examined the UHI, which is maximal from midnight through early morning (Gedzelman et al., 2003), we focus on overall heat stress, which is driven by air temperature, relative humidity, and wind conditions and peaks in the afternoon when human activities are still ongoing.

2. Methodology

2.1. Model description and experiment design

We use WRF model version 4.2.2 with the Advanced Research WRF dynamic core (Skamarock and Klemp, 2008). The model domain is centered at 45.5°N and 85.0°W and has 544 × 485 grid points (2176 km × 1940 km) in the west–east and south–north at a grid spacing of 4 km. The domain covers the Great Lakes region as shown in Wang et al. (2022) Fig. 1. There are 50 stretched vertical levels topped at 50 hPa, with the first 18 levels in the lower 1 km and the first model level 30.2 m above ground level. The initial and boundary conditions are constructed from 3-hourly 0.25° European Centre for Medium-Range Weather Forecasts atmospheric reanalysis of the global climate, version 5 (ERA5; Bell et al., 2020). We use National Oceanic and Atmospheric Administration (NOAA) Great Lakes Surface Environmental Analysis–provided satellite-derived daily lake surface temperature (Schwab et al., 1992) at a spatial resolution of ~1.3 km as a lower boundary condition over the Great Lakes. This dataset was found to be able to produce better results over the Great Lakes region than the default ERA5's sea surface temperature when compared with in situ measurements (Wang et al., 2022). The physics parameterizations include the Rapid Radiative Transfer Model for Global Climate Models longwave and shortwave schemes (Iacono et al., 2008), Mellor–Yamada–Janjic (MYJ) (Janjic, 1990, 1994) planetary boundary layer (PBL) scheme and Monin-Obukhov surface layer scheme, Thompson microphysics (Thompson et al., 2004; Thompson et al., 2008), and Unified Noah land surface model (Noah LSM; Chen and Dudhia, 2001). No sub-grid cloud cover or shallow cumulus parameterizations are used.

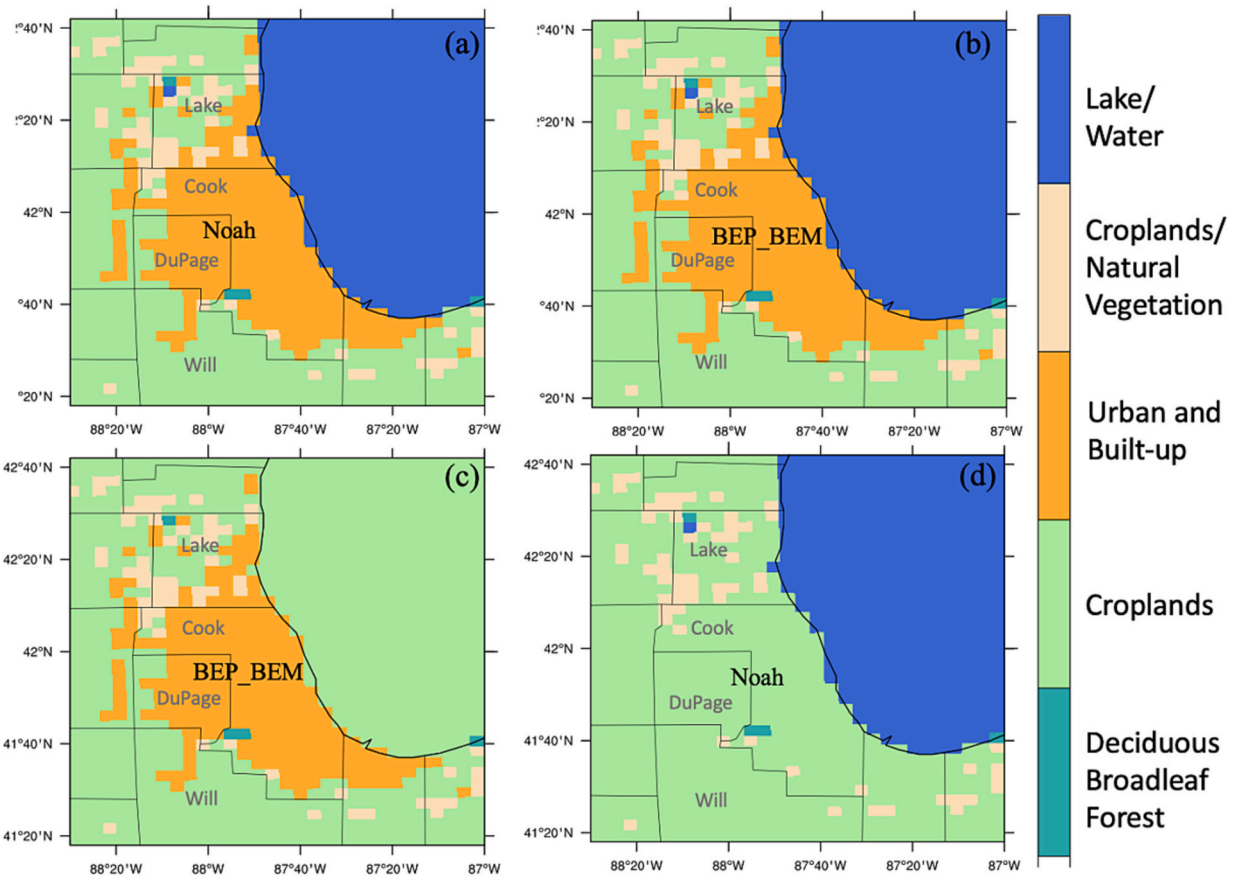

Fig. 2. Studied area: most of the CMA, with the greatest population in Cook and DuPage counties. (a) CTLR: Noah LSM represents zero-order effects of urban surfaces. (b) BEP_BEM: same as CTRL, but coupled with the BEP and BEM. (c) No_LakeM: same as (b) except all of Lake Michigan was replaced by cropland. (d) No_Urban: same as CTRL, except the urban grids over the CMA were replaced by cropland. Note that all the experiments were conducted over the domain shown by Fig. 1 in Wang et al. (2022) at a grid spacing of 4 km with 544 × 485 grid points in the west–east and south–north. Each experiment was run for five ensemble members with different initial conditions. The land-use types over the studied area are based on MODIS 21 land category data.

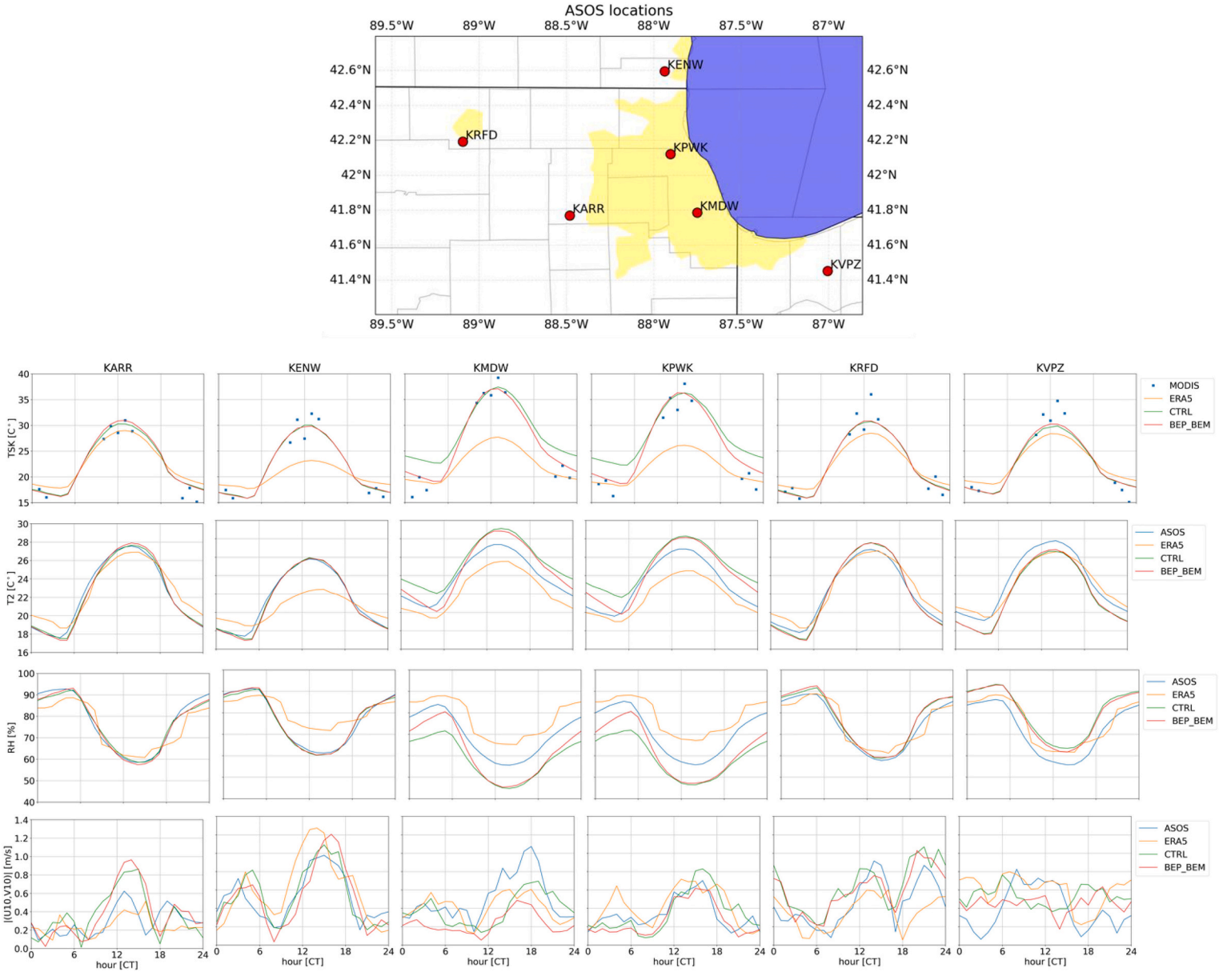

Fig. 3. Model evaluations of diurnal quantities for ERA5, CTRL, and BEP_BEM using six ASOS weather stations. Top: ASOS locations; yellow shading indicates urban area. TSK observations are from MODIS, extracted to the closest point of ASOS locations. Near-surface 2 m air temperature (T2) and relative humidity (RH), and 10 m wind speeds are from ASOS observations. Wind speeds are vector means, $|(U10, V10)|$, across 2018 summer months. (For interpretation of the references to colour in this figure legend, the reader is referred to the web version of this article.)

We performed multiple modeling experiments to examine how urban areas and the lake influence urban heat stress over the CMA. All the experiments were conducted over the entire model domain, as shown in Fig. 1 in Wang et al. (2022), which covers the entire Great Lakes region with 2176 × 1940 km^2, but our study area here is over the CMA, shown in Fig. 2. First, we conducted a simulation using Noah LSM only to treat urban geometry. Noah LSM represents zero-order effects of urban surfaces with increased roughness, decreased soil moisture availability, and decreased albedo (Chen and Dudhia, 2001; Liu et al., 2006; Chen et al., 2011). This experiment is the control simulation, referred to as CTRL experiment in Fig. 2.

Second, to assess the impacts of an undated representation of urban physical processes, we conducted a simulation using WRF coupled with the multilayer urban canopy model BEP and BEM, referred to as the BEP_BEM experiment in Fig. 2. BEP introduced a scheme to represent the impact of urban buildings on resolved airflow (Martilli et al., 2002). It can reproduce the increase of Reynolds stress profiles with height, store more energy in the urban fabric during the day, and reduce the turbulence intensity below the average roof height by changing the length scale (Martilli et al., 2002). BEM was added to BEP to reproduce the generation of heat in buildings and the way heat is exchanged with the exterior flow (Salamanca et al., 2010). BEM considers heat diffusion through walls, roofs, and floors; natural ventilation; the radiation exchange between indoor surfaces; the generation of heat due to occupants and equipment; and the consumption of energy due to air conditioning systems (Salamanca et al., 2010). Our model has air conditioning switched on 24 h a day. The target indoor temperature is 24.85 °C with a comfort range of 0.5 °C. The peak heat generated by other equipment in buildings is estimated as 20 W m^{-2} from 0800 to 1800 local time and 5 W m^{-2} during night. Previous studies have found that using both BEP and BEM can better simulate the UHI during the nighttime, as well as the urban wind speed, compared with the zero-order Noah LSM and the single-layer urban canopy model (Ryu et al., 2016; Wang and Hu, 2021). While Noah LSM can be coupled with any PBL schemes in WRF, BEP_BEM are currently coupled only with three PBL schemes, the MYJ, the Yonsei University PBL scheme (Noh et al., 2003; Hong and Lim, 2006) and the Bougeault–Lacarrére (BouLac) (Bougeault and Lacarrere, 1989). We conducted simulations with BEP_BEM coupled with the YSU PBL scheme and found the bias in air temperature and wind speeds, especially during afternoon to evening, are larger than that produced by BEP_BEM coupled with MYJ PBL.

Third, to examine the effects of urban–nonurban land-use contrast, we replaced the urban land-use within the studied area (the urban grids within CMA, Fig. 2) with cropland. We refer to this simulation as the No_Urban experiment; that is, no urban land use is present in the CMA, so the Noah LSM is applied to the cropland grids over the original urban grids within CMA. Last, to assess the influence of land–lake contrast, we replaced all of Lake Michigan with cropland, which is the adjacent land-use type near southwestern Lake Michigan. We refer to this simulation as the No_LakeM experiment. For the No_LakeM experiment, both urban grids as well as the BEP and BEM treatment were still in place. Notaro et al. (2013) filled the five lakes with surrounding land use types (forest/field mosaic) in a regional climate model, and found the lakes can reduce the amplitude of the diurnal cycle and annual cycle of air temperature year round. However, they did not investigate the contrasting effects from urbanization and lake breeze on variables related to heat stress.

The land-use types over the studied area included urban and built-up areas, croplands, water, cropland/natural vegetation mosaic, and deciduous broadleaf forest based on the Moderate Resolution Imaging Spectroradiometer (MODIS) 21 land category data. Current versions of WRF use this MODIS land-use data by default, and the fraction of the urban landscape that does not have natural vegetation is set to 0.9 for all urban grids. We use 'high density residential' as the default urban category with 20% of building heights at 10 m, 60% at 15 m, and 20% at 20 m. These parameters are reasonable comparing with the local climate zone data based on World Urban Database and Access Portal Tools (Ching et al., 2018, 2019), which shows the majority of the Chicago urban grids belong to open low residential and compact low residential, with building height at 17.5 and 6.5 m, respectively. To ensure the robustness of the conclusion of this study, we conducted an ensemble of 5 members for each of the four experiments shown in Fig. 2. The five members were started with initial conditions 12 h apart between 0000 UTC on 12 May 2018 and 0000 UTC on 14 May 2018, and they all ended on 0000 UTC 1 September 2018. Therefore, the five members overlapped for all of the summer of 2018, with a spin-up period varying from 17 to 19 days. All the results shown in this study is the five-member ensemble mean from June to August 2018. In fact, we found that each single member reports similar conclusions, indicating the small perturbations arising from the different initial conditions do not change the conclusions drawn from this particular study.

2.2. Data and methods

2.2.1. Observations for model evaluation

Six in situ observation sites (Fig. 3) from the Automated Surface Observing System (ASOS) were used to evaluate near-surface air temperature (Ta), relative humidity (RH), and winds from ERA5, CTRL, and BEP_BEM. ASOS instruments are primarily located at airports, because the primary function of the ASOS is to provide minute-scale observations and generate basic aviation weather reports (Nadolski, 1992). We retrieved 5 min air and dew point temperature, and 10 m wind speed and directions, and reduced these to hourly averaged values to match our hourly WRF output.

Among the six locations, three (KPWK, KMDW, and KRFD) are located over urban areas, according to MODIS land type data. Among the three urban locations, two (KPWK and KMDW) are located over the highly urbanized area of the CMA. Another three locations (KENW, KARR, and KVPZ) are located over cropland or natural vegetation according to MODIS land type; KENW and KARR are particularly close to the urban area, which could be influenced by urbanization. We also evaluated skin temperatures (TSK) using MODIS AQUA and TERRA satellite data by picking the overlapping pixels for each ASOS location. These satellite data are available on a semi-diurnal cycle so that we have four readings per day for all days of summer 2018. Last, in situ NOAA National Data Buoy Center's (NDBC's) observations over five selected locations nearshore of Lake Michigan (Fig. S1) were used to evaluate the performance of the ERA5, CTRL, and BEP_BEM experiments in lake surface temperature, Ta, RH, and winds over Lake Michigan.

2.2.2. Heat stress metrics

We focus on heat stress instead of just air temperature because heat stress is a better indicator of thermal discomfort, since it considers both temperature and relative humidity (Sarangi et al., 2021). In addition, the lake and urbanization affect not only on air temperature, but also humidity and wind conditions (Chakraborty et al., 2022). Therefore, we choose three different heat stress metrics that take into account different meteorological factors and have different responses to temperature and relative humidity changes: First, we applied the equation used by the National Weather Service (Rothfusz, 1990; Steadman, 1971; Steadman, 1979) to estimate HI values for the following four conditions. HI is a metric that represents the human perceived temperature by considering the impact of humidity. Sarangi et al. (2021) found that the magnitude of HI is 3–5 times more sensitive to air temperature change than to relative humidity change.

HI_1 is first calculated as a baseline, following Eq. (1):

$$HI_1 = 0.5 \times [T_a + 61.0 + (T_a – 68.0) \times 1.2 + RH \times 0.094] \quad (1)$$

where T_a is in degrees Fahrenheit, and RH is a percentage. If $(HI_1 + T_a)/2 < 80$ °F, then HI_1 is the final HI. If $(HI_1 + T_a)/2 \geq 80$ °F, then HI_2 is calculated as following Eq. (2):

$$\begin{aligned} HI_2 = &-42.379 + 2.04901523 \times T_a + 10.14333127 \times RH – 0.22475541 \times T_a \times RH – 6.83783 \times 10^{-3} \times T_a^2 – 5.481717 \times 10^{-2} \times RH^2 \\ &+ 1.22874 \times 10^{-3} \times T_a^2 \times RH + 8.5282 \times 10^{-4} \times T_a \times RH^2 – 1.99 \times 10^{-6} \times T_a^2 \times RH^2 \end{aligned} \quad (2)$$

If RH < 13% and 80 °F ≤ T_a < 112 °F, then HI_2 needs to be adjusted following Eq. (3):

$$HI_3 = HI_2 – (13 – RH) \Big/ 4 \times \sqrt{[17 – abs\,(T_a – 95)]/17} \quad (3)$$

If RH > 85% and 80 °F ≤ T_a < 87 °F, then HI_2 needs to be adjusted following Eq. (4):

$$HI_4 = HI_2 + (RH – 85)/10 \times (87 – T_a)/5 \quad (4)$$

Next, we used two approaches to calculate wet-bulb temperature (Tw), a thermodynamic measure of humidity in the atmosphere and often used in climate studies to describe heat stress (Sherwood, 2018; Raymond et al., 2020; Zhao et al., 2021). One approach was developed by Stull (2011), as shown by Eq. (5):

$$\begin{aligned} T_w = &T_a \times arctan\left[0.151977 \times (RH + 8.313659)^{1/2}\right] + arctan(T_a + RH) – arctan(RH – 1.676331) + 0.00391838 \times (RH)^{3/2} \\ &\times arctan(0.023101 \times RH) – 4.686035 \end{aligned} \quad (5)$$

The other approach, which was developed by Stipanuk (1973), is an iterative approach that returns the wet-bulb temperature given *Ta*, dewpoint temperature (in degrees Celsius) and surface air pressure (in hectopascal). The analyses shown in this study used the approach of Stipanuk (1973). We found conclusion the same when Stull's equation is used.

Wet-bulb global temperature (WBGT), as proposed by Yaglou and Minard (1957), is calculated as another discomfort index. WBGT is a weighted average of air temperature, natural wet-bulb temperature and black globe temperature. Black globe temperature is a function of radiant heat, air temperature, and air velocity. By incorporating black globe temperature, WBGT considers radiation effects as well as wind effects, whereas many other simplified thermal comfort indices do not (Heo et al., 2019). In our study, both the urbanization and the lake presence would significantly affect the wind speeds. Therefore, it is important to take into account all these factors when investigating the urbanization and lake effects on heat stress over CMA, as in Eq. (6):

$$WBGT = 0.735 \times T_a + 0.0374 \times RH + 0.00292 \times T_a \times RH + 7.619 \times SR – 4.557 \times SR^2 – 0.0572 \times WS – 4.064 \quad (6)$$

where SR and WS are solar insolation (kilowatts per meter) and wind speed (meters per seconds), respectively. T_a is in degrees Celsius.

3. Results

3.1. Model evaluation

Fig. 3 compares ERA5, CTRL, and BEP_BEM simulated and ASOS observed diurnal variation of TSK, *Ta*, RH, and 10 m windspeeds over six selected ASOS locations across the studied area, for 5-member ensemble and three-month mean. The BEP_BEM provides improvement over CTRL in the diurnal range of TSK over the urban locations (RMSE reduced from 5.19 and 5.26 °C to 2.52 and 2.44 °C at KMDW and KPWK, respectively during nighttime. Improvement by BEP_BEM is also found in T_a during early morning, with RMSE reduced from 1.78 and 2.38 °C to 1.02 and 1.52 °C at KMDW and KPWK, respectively, from 18 to next 5 Central Daylight Time (CDT; Table S1).

In addition, BEP_BEM captures the difference between T_a and TSK more realistically than does CTRL. For example, in CTRL, the T_a is always cooler than TSK; in BEP_BEM, however, the T_a is cooler than TSK during the day (by up to 8 °C), but warmer than TSK during the night (1–2 °C) because the BEP_BEM considers the anthropogenic heat impacts on the air, which warm the air temperature overnight. Such discrepancies between T_a and TSK were also found by other studies using satellite and in situ observations despite the land-use types (Jin et al., 1997; Prakash et al., 2019). The overestimation of Ta by CTRL during both day and night was also observed

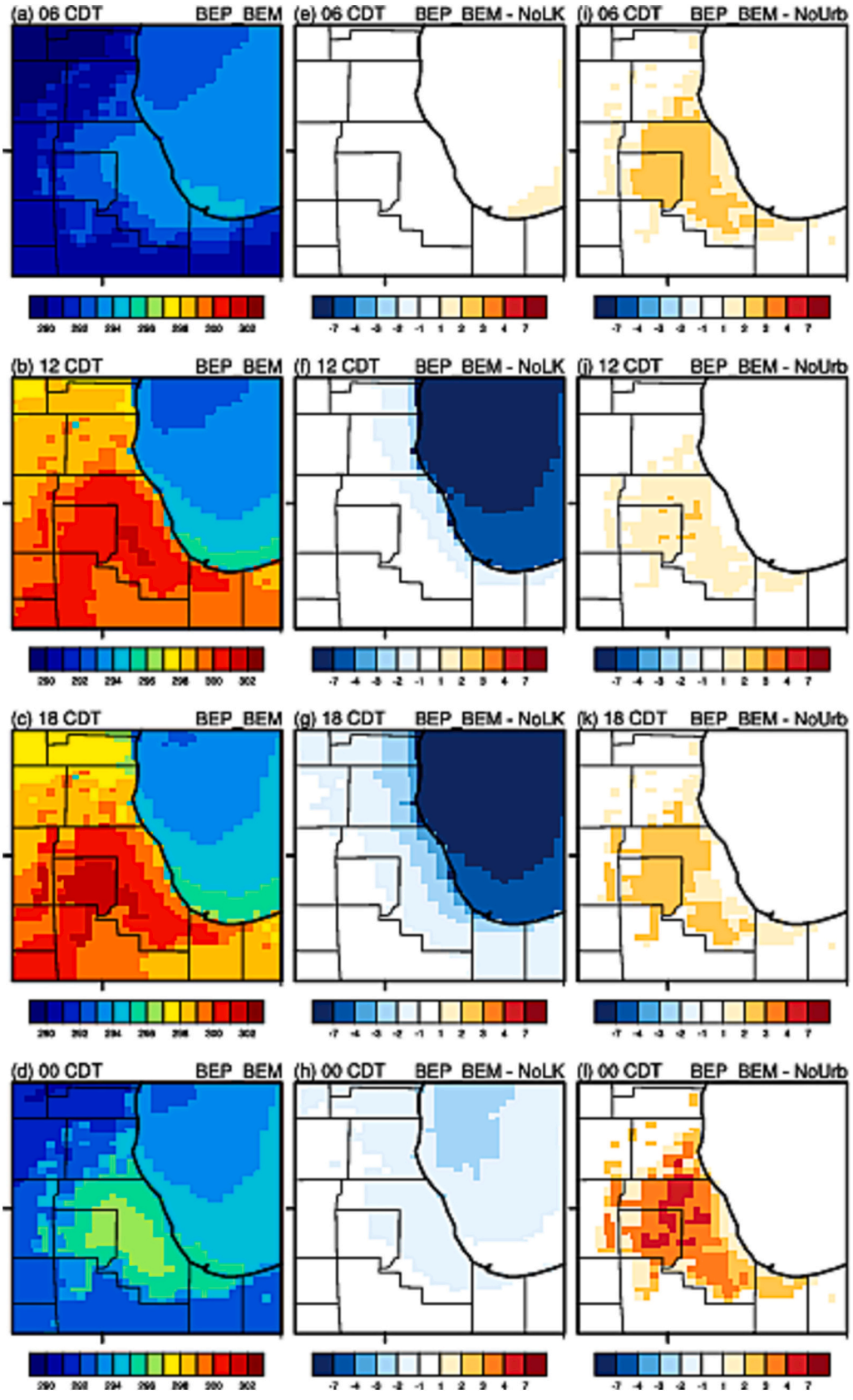

(caption on next page)

Fig. 4. BEP_BEM simulated air temperature at 2 m (a-d); air temperature difference between BEP_BEM and No_LakeM (e-h); and between BEP_BEM and No_Urban (i-l). All results are calculated based on June–August five-ensemble mean.

by Wang and Hu (2021) when comparing two similar model setups as we designed here over Dallas–Fort Worth during a dry summer and a wet summer. Because CTRL and BEP_BEM perform similarly over non-urban areas, the improvement of T_a by BEP_BEM over urban location also helps capture the UHI more realistically.

While both BEP_BEM and CTRL underestimate the 2 m RH, BEP_BEM has larger RH in the morning, closer to the ASOS observations (RMSE reduced from 10.73 to 11.34% to 7.8–8.6% throughout the day) over the two urban locations. This is likely because the T_a is decreased and latent heat flux is increased by BEP_BEM during the same time period, which reduces the moisture capacity but increases the evaporation and can potentially increase RH. For the 10 m wind speeds, all ASOS locations over the western side of Lake Michigan show higher wind speeds in the afternoon and lower wind speed from midnight to morning. Both CTRL and BEP_BEM capture this diurnal pattern over most of the stations except over KVPZ, but BEP_BEM tends to overestimate the wind speeds over the non-urban stations KARR, while underestimating the wind speeds over the urban station KMDW, resulting in a similar agreement with observations (Table S1).

It is noteworthy that Wang and Hu (2021) also found reduced wind speed when using BEP_BEM, but those wind speeds are closer to observations than CTRL. This is because the CTRL experiment uses a roughness length that is not directly dependent on urban morphology, while BEP_BEM estimates the momentum sink with a drag force that depends on urban morphology (Salamanca et al., 2011). Moreover, the Noah LSM used by CTRL is separated from the atmosphere above and communicates with the above atmosphere only with bulk surface flux and grid scale roughness length, while BEP_BEM allows buildings to protrude into the lower atmosphere and is more direct and realistic in capturing building drag effects. The larger discrepancy in our case between the ASOS observation and BEP_BEM simulation is likely due to the following: (1) the ASOS observations are located at airports, with a more open landscape than the urban morphology that WRF assumed in the BEP_BEM experiment, with building heights at least 10 m high, which can potentially reduce wind speeds; (2) the ASOS data is derived from 5 min scale observations, which are more likely to capture very high wind speeds than the hourly output from our WRF simulations. We did find though, using MYJ PBL coupled with BEP_BEM reduced some of the bias in wind speeds over both rural and urban stations, and it reduced the bias in air temperature and relative humidity over urban stations during evening (Table S1), when comparing with BEP_BEM coupled with YSU PBL.

Compared to ERA5, the WRF models clearly show a large improvement in the diurnal range of both TSK and T_a, especially over urban area. One of the reasons is that ERA5 (and most reanalysis datasets) does not explicitly represent urban climate processes, and is not able to reproduce the observed UHI (Chakraborty et al., 2021). Nogueira et al. (2022) demonstrated this limitation of ERA5 over a

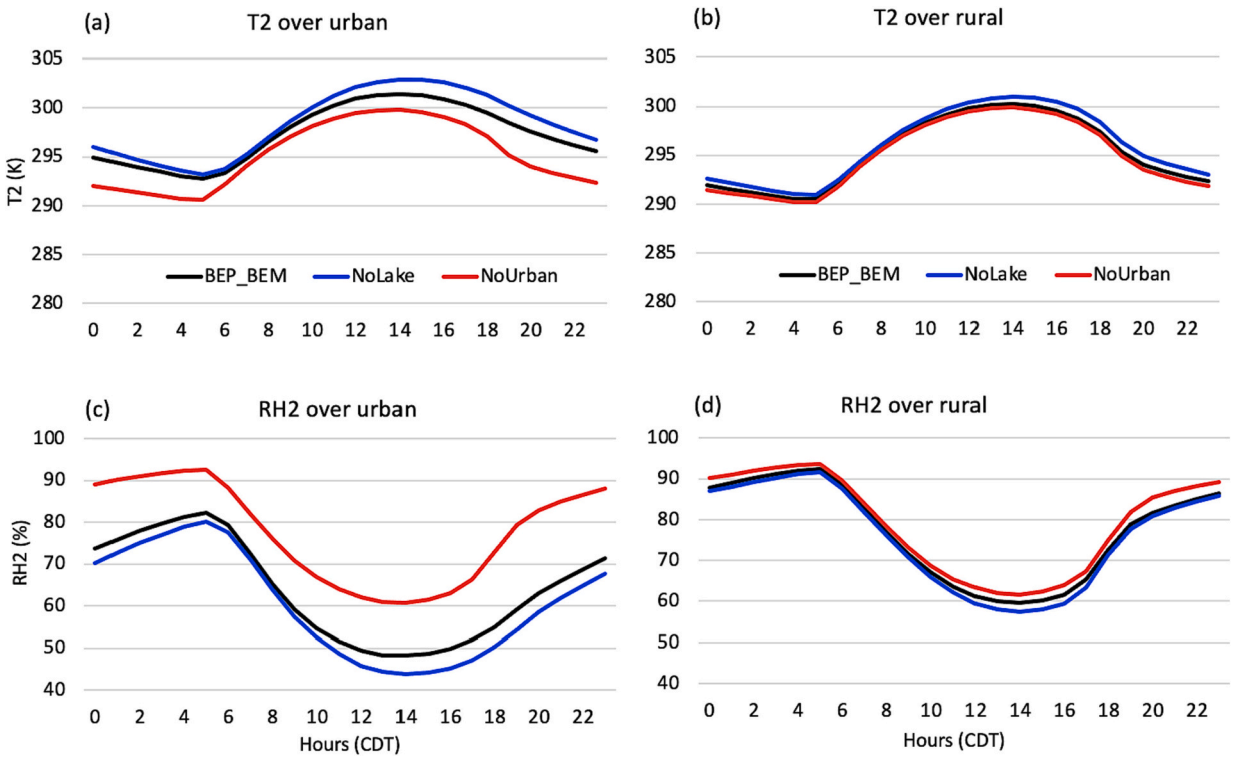

Fig. 5. BEP_BEM, No_Urban, and No_LakeM simulated 2 m air temperature (a, b) and relative humidity (c, d) over urban grids (left) and non-urban grids (right) shown in Fig. 2 and Fig. 4. All results are calculated based on June–August five-ensemble mean.

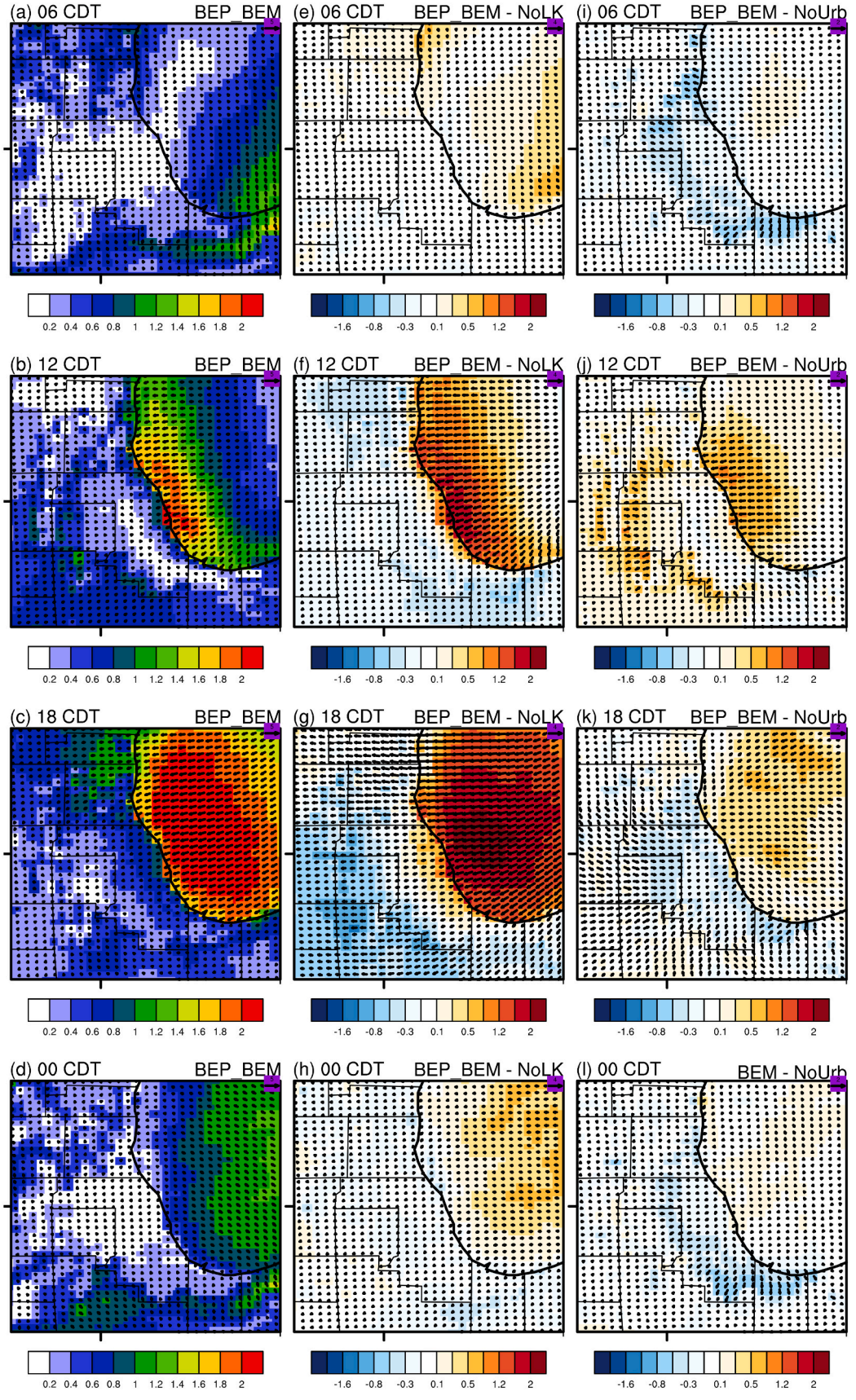

(caption on next page)

Fig. 6. BEP_BEM simulated wind speed (shadings) and direction (arrows) at 10 m (a-d); their differences between BEP_BEM and No_LakeM (e-h); and differences between BEP_BEM and No_Urban (i-l). All results are calculated based on June–August five-member ensemble mean. Note that the reference length of wind arrow is 4 m/s for the middle panel and 2 m/s for the right panel.

mega-city of Paris with strong UHI: ERA5 always showed larger bias over urban grids than over vegetation grids for daily maximum and minimum air temperature. Neither can ERA5 reproduce the diurnal cycle of land surface temperature; it underestimated temperatures by 5 °C, similar to our results here.

Although the daily averaged temperature and winds are reasonably captured by both WRF and ERA5, ERA5 shows quite different diurnal cycles of both temperature and winds at the coastal lake buoys (Fig. S1). The performance of WRF models is also less favorable over buoys than over ASOS locations, especially over locations that are close to the shoreline; none of the models or ERA5 are capable of capturing the diurnal cycle or the magnitude of temperature and wind speeds. One of the reasons for this is that the lake surface temperature used as a lower boundary condition for WRF is at a daily scale and therefore cannot capture the diurnal cycles over the lake. The particularly large bias over shore locations could be related to the resolution of the surface forcing, which may have a larger discrepancy near the coast, motivating the use of coupled model system with a 3-dimensional lake model (e.g., Xue et al., 2017; Sun et al., 2020) to better prescribe the coastal lake surface in future studies.

3.2. Impacts of Lake Michigan and urbanization

In Sect. 3.2.1 we start by analyzing the changes in T_a due to urbanization and lake effects, because the temperature difference across various landscapes drives the wind conditions such as lake breeze, which in turn influences the geospatial patterns of air temperature and moisture. Wind condition (Sect. 3.2.2) and RH (Sect. 3.2.3) changes are presented next to examine their influence on heat stress (Sect. 3.2.4).

3.2.1. Air temperature

Fig. 4 shows 2 m T_a simulated in BEP_BEM, and the difference in T_a between BEP_BEM versus No_LakeM, and between BEP_BEM versus No_Urban over the studied area as shown in Fig. 2 at four local times (06, 12, 18, and 00 CDT). In the BEP_BEM experiment (Fig. 4a-d), the lake-land temperature gradient is large, and there is a strong diurnal cycle of T_a with an increase from morning, reach the highest point in the afternoon (16 CDT; some locations over DuPage County reach a summer average of ~29 °C). The highest T_a is over DuPage County (during afternoon to evening) instead of Cook County, which has the highest population (40% of Illinois) and is the most urbanized (compared with surrounding areas). This is because the lake breeze (Sect. 3.2.2) is the strongest during this time and its propagation toward the land advects the heat farther southwest.

When the lake is filled by cropland, the temperature gradient between the original lake body and urban area is largely reduced, and T_a is warms by 1–2 °C over inland grids and 3–4 °C near shore. The warm core over the urban area not only intensifies and expands but also moves to Cook County (closer to the lake) and lasts longer (Fig. S2). Therefore, as shown in Figs. 4 and 5, the lake presents a cooling effect on T_a throughout the day, first along the shoreline when the lake breeze starts forming, and then expanding farther west with stronger lake breeze in the afternoon. The strongest cooling (4 °C near shore and 1–2 °C inland, ~40 km away from the lake) occurs in the late afternoon (18 CDT for example), when the air temperature is still high and the land-lake temperature difference is the largest. The cooling effect of Lake Michigan on the skin temperature shows a similar diurnal pattern, but with a smaller magnitude and affected area.

When the urban grids are replaced with cropland, the lake-land temperature gradient is also reduced, but not as much as that in the No_LakeM experiment. T_a is reduced throughout the day over both urban and rural grids, and there is no warm island over the studied area (Fig. S2). Therefore, as shown in Figs. 4 and 5, the urbanization creates a warming effect on T_a throughout the day, mostly over the inland urban grids. The largest warming in T_a occurs in the late evening to midnight (21 CDT to 00 CDT), with up to 6 °C warming over many locations in DuPage County and locations away from the lake in Cook County. The urban impacts on skin temperature are of smaller magnitude than the impacts on air temperature, but with similar diurnal pattern: larger in midnight to early morning and smaller around noon.

Comparing the competing impacts of lake and urbanization on air temperature, as shown in Fig. 5 (a-b), the lake's cooling effect is at its highest in late afternoon to early evening (16–19 CDT), while the urban warming effect is in late evening to midnight (19–23 CDT). This means that the strongest warming effect (~3.5 °C) posed by urbanization can be reduced only slightly by the lake (~1.5 °C). Such contrasting impacts from urbanization and lake breeze also exist over non-urban (mainly cropland and natural vegetation) grids, but are much smaller.

3.2.2. Winds

For CMA, winds caused by lake breeze and urban-induced circulations in summer contribute to the ventilation of the city and play an important role in the spatial evolution and magnitude of the heat stress. Fig. 6 shows the 10 m wind conditions (speed and direction) simulated in BEP_BEM, the difference between BEP_BEM versus No_LakeM, and the difference between BEP_BEM versus No_Urban over the studied area. It should be noted that 10 m winds are within the urban canopy, however, simulated winds above the canopy (e.g., at 50 m) are qualitatively similar, suggesting our results are not affected strongly by this choice.

In the BEP_BEM experiment, we see a strong diurnal cycle of wind conditions with slow wind speeds (monthly average <0.1 m/s over some locations in both land and lake) during the nighttime through morning, and strong wind speeds (monthly average >3 m/s)

along the lakeshore and over the lake starting from 11:00 CDT, and then extended to a larger area in the afternoon and last until midnight (00:00 CDT). There is also a change in wind directions from westerly in the morning to easterly in the afternoon. This direction change – specific to the western side of Lake Michigan – is due to the lake breeze (Laird et al., 2001); the lake breeze over the eastern side of Lake Michigan mirrors the western side, as the temperature gradients are opposite.

When the Lake Michigan is filled with cropland (No_LakeM experiment), the diurnal cycle of winds is much weaker compared to the BEP_BEM simulations. The wind speeds are reduced by up to 2 m/s in afternoon and ~ 0.5 m/s throughout the day, and the wind directions over both lake and land (both urban and rural) remain westerly most of the day. However, because there is almost no difference in air temperature between the urban area and the filled lake, the temperature gradient between rural and urban dominates and promotes rural breeze in the afternoon blowing from rural to urban (Fig. S3). When the urban is replaced by cropland (No_Urban experiment), the lake breeze still develops, initiating around noon and reach the peak at 18 CDT. The wind speeds are slower over the lake, because the temperature gradient is smaller between lake and cropland than that between lake and urban. When the urban landscape is excluded, the wind speeds are faster over the land, especially over the locations originally specified as urban (Fig. S3), presumably because the frictional effects of the urban canopy are now absent.

In summary, the presence of the lake increases the wind speed over lake and causes the wind direction shift from morning to afternoon (Figs. 6 and 7), bringing the cool air from lake to lands; however, the presence of the lake also decreases the wind speeds over sub-urban and rural areas. This is because the penetration of lake breeze cancels out some westerly wind due to “rural breeze”, which opposes the lake breeze. Urbanization also increases the wind speeds over lake, particularly along the lake shore, due to increased thermal gradients. However, it decreases the wind speeds over urban area, because of increased drag effect due to the urban canopy, which has a surface roughness much larger than cropland, making the lake breeze penetration more difficult. There may also be some compensating effects due to the rural breeze mentioned above, however, it is difficult to ascertain if this effect is stronger than the increase in lake breeze due to elevated urban temperatures. These findings are consistent to Ribeiro et al. (2018). In contrast, urbanization increases the wind speed over rural areas around noon because of the temperature gap between rural and urban areas, which causes stronger westerly and southwesterly wind from rural areas to urban areas (Oke, 1995). The increased westerly wind toward the CMA together with the easterly lake breeze form a convergence over the urban area, which can potentially maintain the UHI longer.

To better understand how lake and urbanization affect individual events, we selected a typical lake breeze event with an UHI signal over CMA on June 7, 2018 (Fig. S4). We found the lake breeze penetration is slower over urban grid than that over sub-urban and rural areas, agreeing with previous case studies (Freitas et al., 2007; Keeler and Kristovich, 2012; Ribeiro et al., 2018) as well as our seasonal and ensemble mean, as shown in Figs. 6 and 7. The lake breeze on the eastern side of Lake Michigan penetrates into the land (mainly cropland, no urban) at a faster and more steady speed. Similar penetration speed is seen when the urban is replaced with cropland for CMA. In addition, we selected four locations with same distance to each other but are over lake, urban, suburban and rural areas, and investigated their air temperature and PBL height variations throughout the day. We found that, the sub-urban air temperature dropped three hours later than did the urban air temperature, while the rural air temperature dropped only one hour later than the suburban air temperature (Fig. S5). This indicates that the lake breeze propagates through urban regions much slower than it does through suburban and rural regions, meaning the lake breeze reached the Chicago suburbs much later than it reaches the urban area closer to the lake, such that cooling over suburbs is relatively delayed; as a result, the suburbs have the highest air temperature in the afternoon compared with other spatial locations over CMA. For this particular event, based on the timing of air temperature decreases at each location, we estimated the lake breeze penetration speed is 2.37 m/s over urban, similar to Freitas et al. (2007) and Ribeiro et al. (2018); and is 6.94 m/s over rural, faster than previous studies (e.g., Ribeiro et al., 2018 and their references; 3–4 m/s) probably due to the smaller drag effect of cropland. When urban grid points are replaced by cropland, the delay of temperature drop in suburbs is much shorter, indicating the importance of the urban canopy in setting the suburban diurnal temperature signal. When the lake is filled by the cropland, all locations show similar variations of air temperature, indicating Lake Michigan is an important driver forming the temperature gradients from urban to rural areas. We also found an abrupt drop in PBL height when the lake breeze front arrives at each location, bringing colder and moister air from the lake and inducing the formation of a thermal internal boundary layer, disrupting the vertical evolution of the boundary layer. Similar to the air temperature, the drop of the PBL height over suburban is three hours later than that over urban regions, while the drop over rural areas is only one hour later than the suburbs, further evidence that the lake breeze is decelerated by urbanization.

3.2.3. *Relative humidity*

Fig. 8 shows 2 m RH simulated in BEP_BEM, and the difference in RH between BEP_BEM versus No_LakeM, and between BEP_BEM versus No_Urban over the studied area. In the BEP_BEM experiment, during late evening to early morning, there is a “dry island” over DuPage and Cook counties because there is less latent heat flux and evaporation over the urban grids. In the No_LakeM experiment, the RH decreases over all land grids. Moreover, the dry island strengthens and expands farther out to rural grids surrounding the lake (Fig. 5 and Fig. S6). This lake-induced increase in RH shows the largest magnitude around 18:00–20:00 CDT, and has the largest area of influence at midnight with slightly smaller magnitude than earlier evening. In the No_Urban experiment, the RH increases over land grids, and the dry island disappears between midnight (by 20%) to early morning because evaporation from croplands is higher than that over the original urban grids (Fig. 5 and Fig. S6). Unlike the lake effects, urbanization impacts have similar areas of influence throughout the day. In addition, urbanization affects RH mostly over inland grids, with the shoreline unchanged, because the lake breeze still exists and can bring in moisture. The drying effects are the strongest around midnight, reducing RH over most of Cook and DuPage counties.

In summary, when the lake shows the largest cooling effect, it also shows the largest increase in RH (e.g., 18:00 CDT) and vice versa

for urban drying and warming effects. Over urban grids, especially the inland urban areas (e.g., DuPage County), RH is reduced by urbanization (5–10% during the day and 15–20% at night) more than it is increased by lake breeze (~8% at most during night). The changes of RH over non-urban (rural) grids are smaller (1–3%) due to the contrasting effects from both urbanization and lake effect (Fig. 5).

3.2.4. Heat stress

The different impacts from urbanization (warming and drying, peak at evening) and the lake breeze (cooling and moistening, peak in late afternoon) on T_a, winds, and RH over CMA, as discussed in Sect. 3.1.1–3.1.3, can influence the heat stress differently. The three heat stress indices defined in Sect. 2.5 (T_w, WBGT, and HI) are presented in this section to demonstrate the different response of heat stress to T_a, RH, and wind speed changes. Because HI's change is dominated by the air temperature change, we see that the impacts from lake and urbanization on HI are similar to their impacts on T_a (Fig. S7). For example, the lake reduces the heat stress with the largest magnitude near shore at 18:00 CDT (by 3–4 °C) and the largest influence area from 18:00 to 00:00 CDT. Urbanization intensifies the heat stress, peaking at midnight (by 4–6 °C) with an influence area mostly over urban grids (e.g., Cook and DuPage counties).

Fig. 9 (a-c) shows the diurnal cycle of T_w, WBGT, and HI in the three experiments. In general, heat stress is the worst during the afternoon. The lake starts reducing heat stress from morning (8:00–10:00 CDT), and maximizes the impacts in the late afternoon and early evening (19–20:00 CDT). The largest impacts of urbanization on heat stress (intensification) are mainly seen during evening. We also examined the lake and urban impacts on urban heat stress island (UHSI), calculated by subtracting the rural heat stress from the urban heat stress in each of the three experiments (Fig. 9d). Comparing the three indices, we see that HI is warmed up (cooled down) by

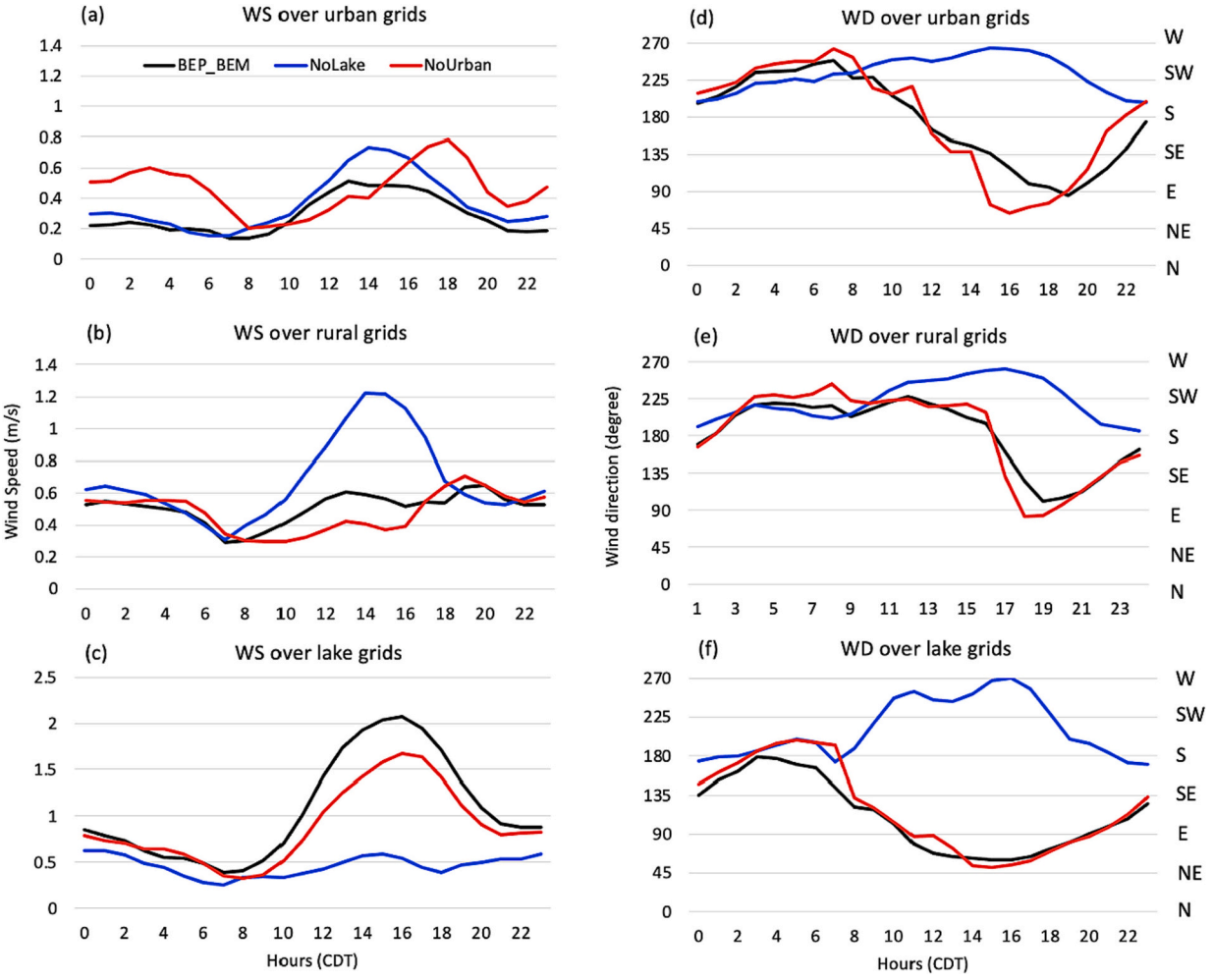

Fig. 7. Wind speed (a-c) and direction (d-f) over urban grids, non-urban land grids (e.g., croplands and natural vegetation) and lake grids, respectively, as shown in Fig. 2. The wind direction is defined as the direction from which it originates, and is measured in degrees clockwise from due north. For example, a wind coming from the south has a wind direction of 180°; one from the east is 90°. Over lake grids in afternoon, the wind comes mostly from the east.

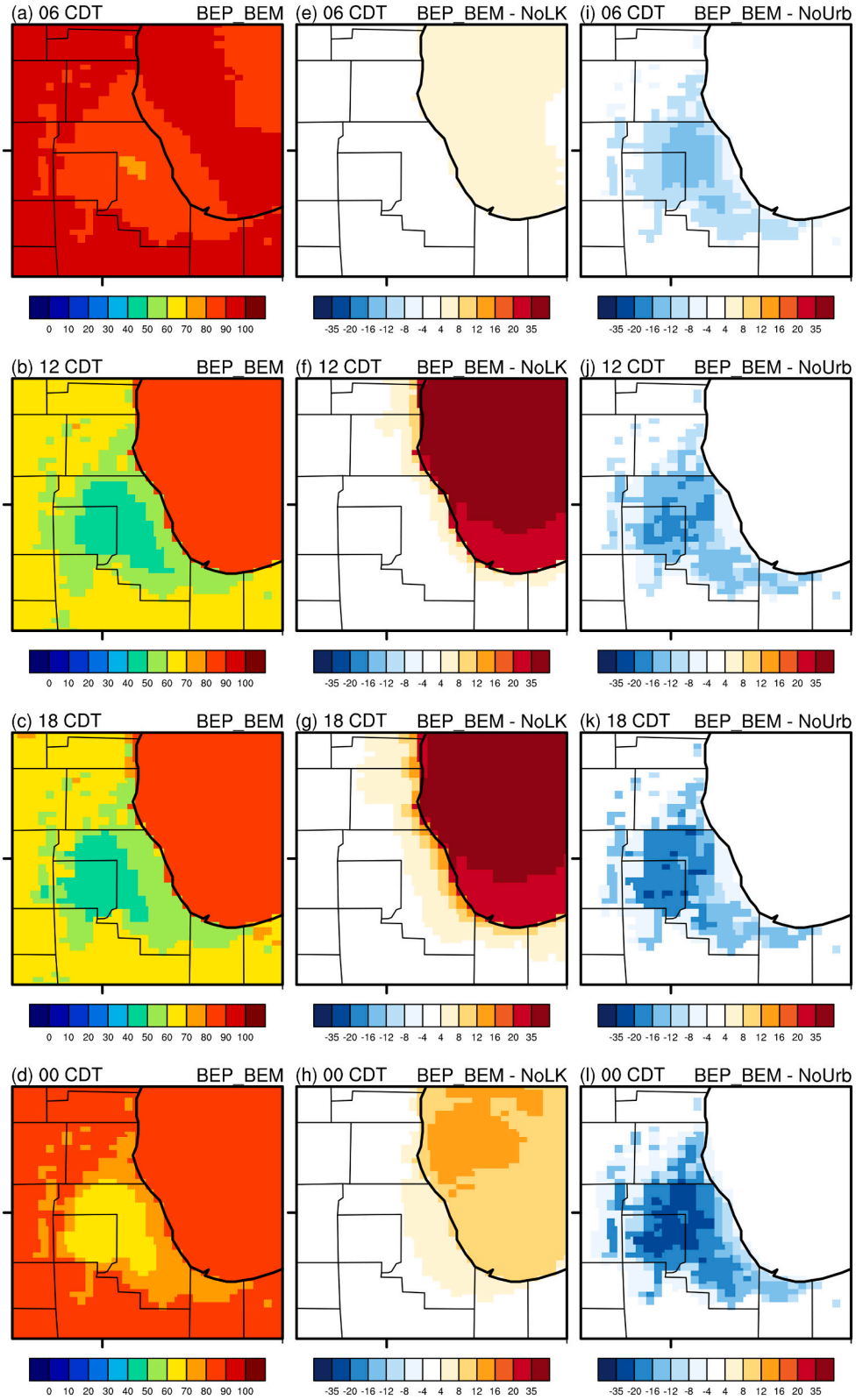

Fig. 8. Same as Fig. 4, but for 2 m RH.

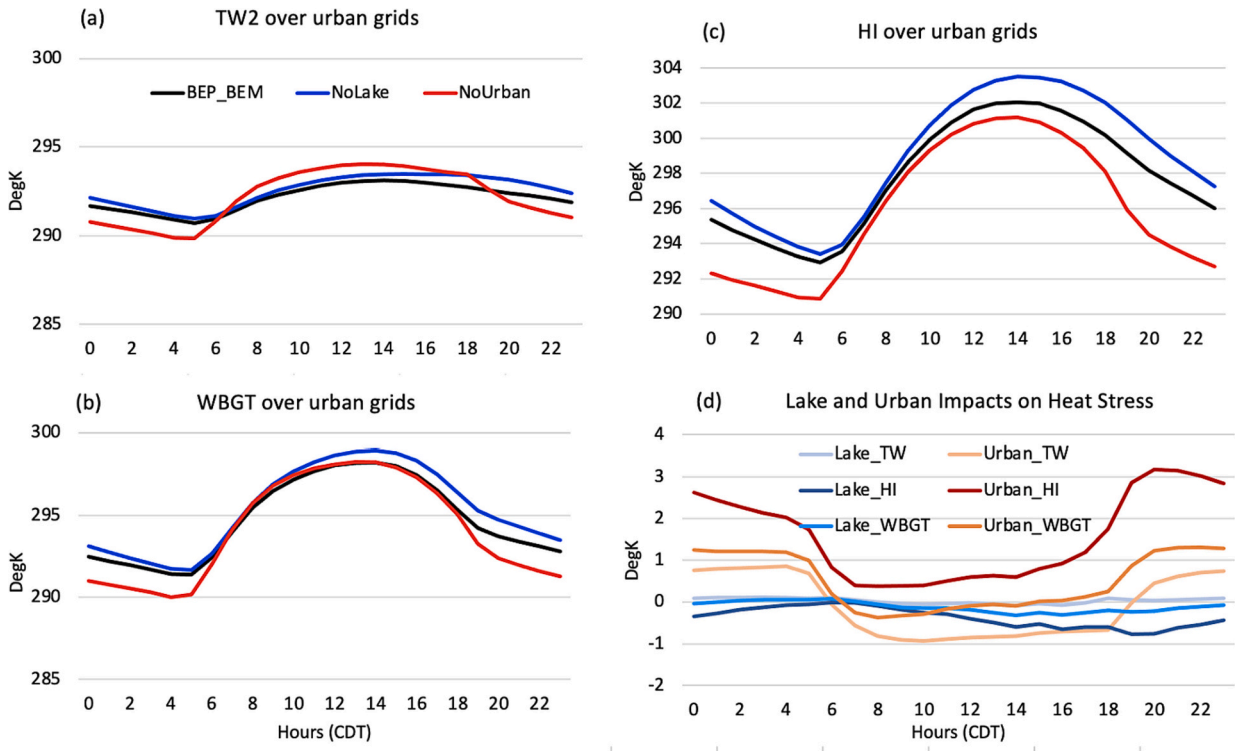

Fig. 9. (a-c) T_w, WBGT, and HI averaged over urban grids shown in Fig. 2. (d) impacts of urbanization versus lake breeze on urban heat stress island (UHSI). The UHSI is calculated by subtracting the rural heat stress from urban heat stress in each experiment using T_w, HI, and WBGT, respectively, as the heat stress index.

urbanization (lake effect) the most, followed by WBGT. Regardless of the indices used, the intensification by urbanization is >4 times larger than the reduction by the lake during late afternoon to evening. The urbanization impact on T_w during the daytime is an exception, because T_w is more sensitive to RH (compared to T_a), and urbanization reduces the RH more than it increases the T_a (Fig. 5), therefore the heat stress described by T_w is reduced by urbanization.

We also counted the heat caution hours (HCH, defined by the number of hours per day with HI > 27 °C or 80.6 °F; Sarangi et al., 2021) in the three experiments to quantify the impacts of lake and urbanization on extreme heat stress conditions (Fig. 10). The presence of the lake can reduce HCH by up to 4 h per day near lakeshore, and 1–3 h per day over the majority of Cook County and Lake County, and by 1–2 h per day over half of DuPage County. These reductions in HCH most likely occur in the afternoon when the lake

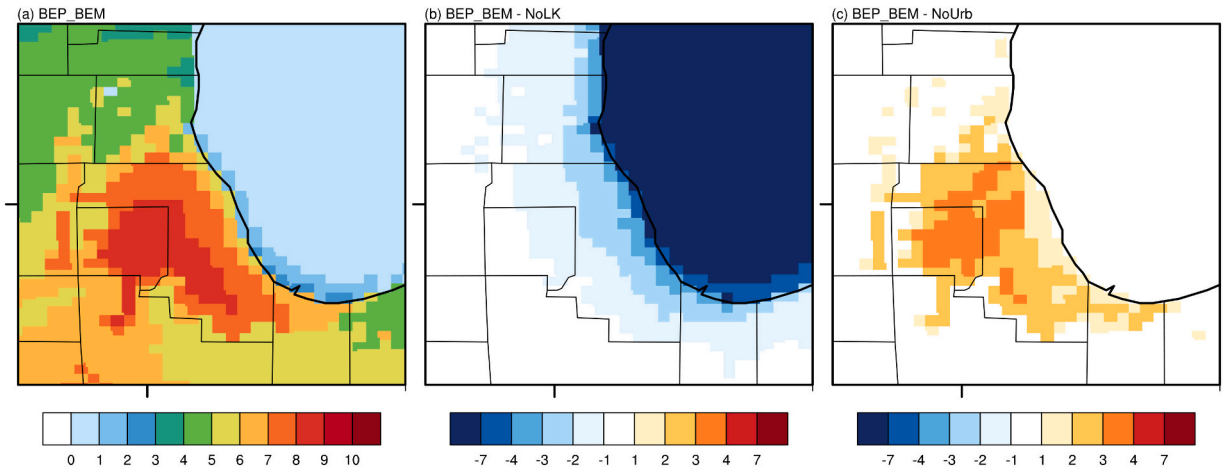

Fig. 10. (a) BEP_BEM simulated heat caution hours (HCH) per day, calculated based on number of days with HI >27 °C. (b-c) difference in HCH between BEP_BEM versus No_LakeM, and between BEP_BEM versus No_Urban.

cooling is the strongest. In contrast, urbanization increases HCH over most of Cook and DuPage counties and half of Lake County (by 2–4 h per day). Near-shore enhancements are restricted to 1 h per day. The largest increase of HCH is over DuPage County – up to 4 h per day (Fig. 5), clearly demonstrating the urbanization-induced increases in duration of extreme heat stress.

4. Summary and discussion

Using the latest WRF model coupled with multilayer urban canopy models (BEP and BEM), we investigated the interaction and contrasting impacts from urbanization and lake breeze on heat stress in 2018 summer over the CMA. Our results show that the WRF coupled with BEP_BEM can better capture the diurnal cycle and the diurnal range of surface air temperature, skin temperature, and relative humidity. This indicates that, in order to reliably simulate the regional climate at urban scale and its potential impacts on the surroundings, interactions between the urban surface, lake and the atmosphere need to be considered, although the use of urban models coupled to climate models requires higher computational costs (Nogueira et al., 2019). The presence of Lake Michigan enlarges the air temperature gradient between lake and land, causing the lake breeze during afternoon to evening, bringing cool, moist air to the CMA and suburban, and disrupting the vertical evolution of urban boundary layer. The urbanization also enlarges (although not as much as the presence of the lake) the air temperature gradient between lake and urban areas and between rural and urban areas, intensifying the wind speeds over lake, but decelerating the penetration of lake breeze into suburban and rural areas.

Even though WRF coupled with BEP_BEM reasonably captures near-surface urban meteorology, there are still uncertainties to be aware of. The model uses a tiled approach to examine the influence of urban vegetation; the pervious fraction is held constant for all urban grids, which can have an impact on simulated T_a and RH. It is difficult to quantify these uncertainties from evaluations, because there is a mismatch in scale between the model-simulated gridded variables and the in situ observations. Moreover, this tiled approach cannot simulate the shading effect of vegetation within urban canyons (Krayenhoff et al., 2020), which can influence heat stress at the pedestrian scale (Middel et al., 2021). Finally, urban representation in models does not fully capture morphological, radiative, and thermodynamic properties in their full complexity (Garuma, 2018; Qian et al., 2022), which requires finer model resolution and further urban model developments, as well as finer resolution land use/land cover data that can better resolve the urban heterogeneity (Ching et al., 2018, 2019).

Last but not least, we found using a nested domain with two-way feedback can reduce some model bias for air temperature and relative humidity, but it can also bring larger biases for the wind components possibly due to the boundary effects from the nesting, suggesting that a sufficiently large domain size should be considered if nesting approach is used. In addition, the model bias over lake (near shore) is relatively large (compared with inland locations). This could be due to the relatively coarse resolution (although it is convective permitting) setup, which is not sufficient to capture the land–lake mask and/or complex terrain transition. This bias may be improved by coupling a three-dimensional lake model at very high spatial resolutions (Huang et al., 2022). Although those limitations and uncertainties exist, we believe our overall conclusions associated with lake and urbanization effects remain solid and are in line with our conceptual understanding of these interactions and previous studies (Gedzelman et al., 2003; Tan et al., 2009; Meir et al., 2013; Sharma et al., 2017; Sarangi et al., 2021; Qian et al., 2022).

Author contribution

JW participated in the entire project by running ensemble simulations and writing the manuscript. QY designed the experiments and participated the writing. WP collected observation data and conducted model evaluations. TC, ZY, RH and PX participated the discussions through the entire study and co-wrote the manuscript.

Declaration of Competing Interest

The authors declare that they have no conflict of interest.

Data availability

Data will be made available on request.

Acknowledgements

This study is supported by COMPASS-GLM, a multi-institutional project supported by the U.S. Department of Energy, Office of Science, Office of Biological and Environmental Research, Earth and Environmental Systems Modeling program. This material is also based upon work supported by the U.S. Department of Energy, Office of Science, Office of Biological and Environmental Research's Urban Integrated Field Laboratories research activity under contract number DE-AC02- 06CH11357. This work is also Contribution No. 95 of the Great Lakes Research Center at Michigan Technology Univeristy. We sincerely thank Dr. Cenlin He from NCAR and two anonymous reviewers for their valuable comments and suggestions. Computational resources are provided by the DOE-supported National Energy Research Scientific Computing Center. All the calculations are done using the NCAR Command Language (version 6.6.2) [Software]. 2019. Boulder, Colorado: UCAR/NCAR/CISL/TDD. https://doi.org/10.5065/D6WD3XH5. The Pacific Northwest National Laboratory is operated for DOE by Battelle Memorial Institute under contract DE-AC05-76RL01830.

Appendix A. Supplementary data

Supplementary data to this article can be found online at https://doi.org/10.1016/j.uclim.2023.101429.

References

Ackerman, B., 1985. Temporal march of the Chicago heat island. J. Clim. Appl. Meteorol. 24 (6), 547–554. https://doi.org/10.1175/1520-0450(1985)024<0547:TMOTCH>2.0.CO;2.

Anderson, G.B., Bell, M.L., 2011. Heat waves in the United States: mortality risk during heat waves and effect modification by heat wave characteristics in 43 US communities. Environ. Health Perspect. 119 (2), 210–218. https://doi.org/10.1289/ehp.1002313.

Atkinson, B., 2003. Numerical modelling of urban heat-island intensity. Bound.-Layer Meteorol. 109 (3), 285–310. https://doi.org/10.1023/A:1025820326672.

Bell, B., Hersbach, H., Berrisford, P., Dahlgren, P., Horányi, A., Muñoz Sabater, J., Nicolas, J., Radu, R., Schepers, D., Simmons, A., Soci, C., Thépaut, J.-N., 2020. ERA5 hourly data on pressure levels from 1950 to 1978 (preliminary version), Copernicus Climate Change Service (C3S) Climate Data Store (CDS). https://cds.climate.copernicus-climate.eu/cdsapp#!/dataset/reanalysis-era5-pressure-levels-preliminary-back-extension?tab=overview.

Bougeault, P., Lacarrere, P., 1989. Parameterization of orography- induced turbulence in a mesobeta-scale model. Mon. Weather Rev. 117, 1872–1890 https://doi.org/10.1175/1520-0493(1989)117,1872:POOITI.2.0.CO;2.

Chakraborty, T.C., Sarangi, C., Lee, X., 2021. Reduction in human activity can enhance the urban heat island: insights from the COVID-19 lockdown. Environ. Res. Lett. 16 (5), 054060 https://doi.org/10.1088/1748-9326/abef8e.

Chakraborty, T., Venter, Z.S., Qian, Y., Lee, X., 2022. Lower urban humidity moderates outdoor heat stress. AGU Adv. 3 https://doi.org/10.1029/2022AV000729 e2022AV000729.

Chemel, C., Sokhi, R., 2012. Response of London's urban heat island to a marine air intrusion in an easterly wind regime. Bound.-Layer Meteorol. 144 (1), 65–81. https://doi.org/10.1007/s10546-012-9705-x.

Chen, F., Dudhia, J., 2001. Coupling an advanced land surface–hydrology model with the Penn State–NCAR MM5 modeling system. Part I: model implementation and sensitivity. Mon. Weather Rev. 129, 569–585. https://doi.org/10.1175/1520-0493(2001)129<0569:CAALSH>2.0.CO;2.

Chen, F., Kusaka, H., Bornstein, R., Ching, J., Grimmond, C.S.B., Grossman-Clarke, S., Zhang, C., 2011. The integrated WRF/urban modelling system: development, evaluation, and applications to urban environmental problems. Int. J. Climatol. 31, 273–288. https://doi.org/10.1002/joc.2158.

Ching, J., Mills, G., Bechtel, B., See, L., Feddema, J., Wang, X., Ren, C., Brousse, O., Martilli, A., Neophytou, M., Mouzourides, P., Stewart, I., Hanna, A., Ng, E., Foley, M., Alexander, P., Aliaga, D., Niyogi, D., Shreevastava, A., Bhalachandran, P., Masson, V., Hidalgo, J., Fung, J., Andrade, M., Baklanov, A., Dai, W., Milcinski, G., Demuzere, M., Brunsell, N., Pesaresi, M., Miao, S., Mu, Q., Chen, F., Theeuwes, N., 2018. WUDAPT: an urban weather, climate, and environmental modeling infrastructure for the anthropocene. Bull. Amer. Meteor. Soc. 99, 1907–1924. https://doi.org/10.1175/BAMS-D-16-0236.1.

Ching, J., Aliaga, D., Mills, G., Masson, V., See, L., Neophytou, M., Middel, A., Baklanov, A., Ren, C., Ng, E., Fung, J., Wong, M., Huang, Y., Martilli, A., Brousse, O., Stewart, I., Zhang, X., Shehata, A., Miao, S., Wang, X., Wang, W., Yamagata, Y., Duarte, D., Li, Y., Feddema, J., Bechtel, B., Hidalgo, J., Roustan, Y., Kim, Y., Simon, H., Kropp, T., Bruse, M., Lindberg, F., Grimmond, S., Demuzure, M., Chen, F., Li, C., Gonzales-Cruz, J., Bornstein, B., He, Q., Ping, T., Adel, H., Evyatar, E., Tapper, N., Mall, Rk, Niyogi, D., 2019. Pathway using WUDAPT's digital Synthetic City tool towards generating urban canopy parameters for multi-scale urban atmospheric modeling. Urban Clim. 28, 100459 https://doi.org/10.1016/j.uclim.2019.100459.

Conry, P., Fernando, H.J.S., Leo, L.S., Sharma, A., Potosnak, M., Hellmann, J., 2014. Multi-scale simulations of climate-change influence on Chicago Heat Island. In: Proceedings of Fluids Engineering Division Summer Meeting, American Society of Mechanical Engineers, Chicago, Illinois, USA, August 3–7, 2014. https://doi.org/10.1115/FEDSM2014-21581. V01DT28A007.

Conry, P., Sharma, A., Potosnak, M.J., Leo, L.S., Bensman, E., Hellmann, J.J., Fernando, H.J., 2015. Chicago's heat island and climate change: bridging the scales via dynamical downscaling. J. Appl. Meteorol. Climatol. 54 (7), 1430–1448. https://doi.org/10.1175/JAMC-D-14-0241.1.

Dahl, K., Licker, R., Abatzoglou, J.T., Declet-Barreto, J., 2019. Increased frequency of and population exposure to extreme heat index days in the United States during the 21st century. Environ. Res. Comm. 1 (7), 075002 https://doi.org/10.1088/2515-7620/ab27cf.

Ebi, K.L., Meehl, G., 2007. The heat is on: climate change and heatwaves in the Midwest. In: Regional Impacts of Climate Change: Four Case Studies in the United States, 22201, pp. 8–21. https://citeseerx.ist.psu.edu/viewdoc/download?doi=10.1.1.192.1201&rep=rep1&type=pdf.

Freitas, E.D., Rozoff, C.M., Cotton, W.R., Dias, P.L.S., 2007. Interactions of an urban heat island and sea-breeze circulations during winter over the metropolitan area of São Paulo, Brazil. Bound.-Layer Meteorol. 122 (1), 43–65.

Garuma, G.F., 2018. Review of urban surface parameterizations for numerical climate models. Urban Clim. 24, 830–851. https://doi.org/10.1016/j.uclim.2017.10.006.

Gedzelman, S.D., Austin, S., Cermak, R., Stefano, N., Patridge, S., Quesenberry, S., Robinson, D.A., 2003. Mesoscale aspects of the urban heat island around new York City. Theor. Appl. Climatol. 75, 29–42. https://doi.org/10.1007/s00704-002-0724-2.

Grimm, N.B., Faeth, S.H., Golubiewski, N.E., Redman, C.L., Wu, J.G., Bai, X.M., Briggs, J.M., 2008. Global change and the ecology of cities. Science 319, 756–760. https://doi.org/10.1126/science.1150195.

Grimmond, S.U.E., 2007. Urbanization and global environmental change: local effects of urban warming. Geogr. J. 173 (1), 83–88. https://doi.org/10.1111/j.1475-4959.2007.232_3.x.

Heo, S., Bell, M.L., Lee, J.T., 2019. Comparison of health risks by heat wave definition: applicability of wet-bulb globe temperature for heat wave criteria. Environ. Res. 168, 158–170. https://doi.org/10.1016/j.envres.2018.09.032.

Hidalgo, J., Masson, V., Gimeno, L., 2010. Scaling the daytime urban heat island and urban-breeze circulation. J. Appl. Meteorol. Climatol. 49 (5), 889–901. https://doi.org/10.1175/2009JAMC2195.1.

Hong, S.Y., Lim, J.J., 2006. The WRF single-moment 6-class microphysics scheme (WSM6). J. Korean Meteorol. Soc. 42, 129–151. https://www.researchgate.net/profile/Song-You-Hong/publication/331192569_Hongandlim-JKMS-2006/links/5c6b581f92851c1c9dea9d10/Hongandlim-JKMS-2006.pdf.

Hu, X.M., Xue, M., 2016. Influence of synoptic sea-breeze fronts on the urban heat island intensity in Dallas–Fort Worth, Texas. Mon. Weather Rev. 144 (4), 1487–1507. https://doi.org/10.1175/MWR-D-15-0201.1.

Huang, C., Anderson, E., Liu, Y., Ma, G., Mann, G., Xue, P., 2022. Evaluating essential processes and forecast requirements for meteotsunami-induced coastal flooding. Nat. Hazards 110 (3), 1693–1718. https://doi.org/10.1007/s11069-021-05007-x.

Iacono, M.J., Delamere, J.S., Mlawer, E.J., Shephard, M.W., Clough, S.A., Collins, W., 2008. Radiative forcing by long-lived greenhouse gases: calculations with the AER radiative transfer models. J. Geophys. Res.-Atmos. 113 (D13), D13103. https://doi.org/10.1029/2008JD009944.

Janjic, Z.I., 1990. The step-mountain coordinate: physical package. Mon. Weather Rev. 118, 1429–1443. https://doi.org/10.1175/1520- 0493(1990)118,1429:TSMCPP.2.0.CO;2.

Janjic, Z.I., 1994. The step-mountain eta coordinate model: further developments of the convection, viscous sublayer, and tur- bulence closure schemes. Mon. Weather Rev. 122, 927–945. https://doi.org/10.1175/1520-0493(1994)122,0927:TSMECM. 2.0.CO;2.

Jin, M., Dickinson, R.E., Vogelmann, A.M., 1997. A comparison of CCM2–BATS skin temperature and surface-air temperature with satellite and surface observations. J. Clim. 10 (7), 1505–1524. https://doi.org/10.1175/1520-0442(1997)010<1505:ACOCBS>2.0.CO;2.

Karl, T.R., Knight, R.W., 1997. The 1995 Chicago heatwave: how likely is a recurrence? Bull. Amer. Meteorol. Soc. 78, 1107–1119. https://doi.org/10.1175/1520-0477(1997)078<1107:TCHWHL>2.0.CO;2.

Keeler, J.M., Kristovich, D.A., 2012. Observations of urban heat island influence on lake-breeze frontal movement. J. Appl. Meteorol. Climatol. 51 (4), 702–710. https://doi.org/10.1175/JAMC-D-11-0166.1.
Krayenhoff, E.S., Jiang, T., Christen, A., Martilli, A., Oke, T.R., Bailey, B.N., Nazarian, N., Voogt, J.A., Giometto, M.G., Stastny, A., Crawford, B.R., 2020. A multi-layer urban canopy meteorological model with trees (BEP-tree): street tree impacts on pedestrian-level climate. Urban Clim. 32, 100590 https://doi.org/10.1016/j.uclim.2020.100590.
Kunkel, K.E., Changnon, S.A., Reinke, B.C., Arritt, R.W., 1996. The July 1995 heat wave in the Midwest: a climatic perspective and critical weather factors. Bull. Am. Meteorol. Soc. 77 (7), 1507–1518. https://doi.org/10.1175/1520-0477(1996)077<1507:TJHWIT>2.0.CO;2.
Laird, N.F., Kristovich, D.A., Liang, X.Z., Arritt, R.W., Labas, K., 2001. Lake Michigan lake breezes: climatology, local forcing, and synoptic environment. J. Appl. Meteorol. 40 (3), 409–424. https://doi.org/10.1175/1520-0450(2001)040<0409:LMLBCL>2.0.CO;2.
Liu, Y., Chen, F., Warner, T., Basara, J., 2006. Verification of a mesoscale data-assimilation and forecasting system for the Oklahoma City area during the joint urban 2003 field project. J. Appl. Meteorol. Climatol. 45 (7), 912–929. https://doi.org/10.1175/JAM2383.1.
Martilli, A., Clappier, A., Rotach, M., 2002. W.: an urban surface exchange parameterisation for mesoscale models. Bound.-Layer Meteorol. 104 (2), 261–304. https://doi.org/10.1023/A:1016099921195.
Meehl, G.A., Tebaldi, C., 2004. More intense, more frequent, and longer lasting heat waves in the 21st century. Science 305 (5686), 994–997. https://doi.org/10.1126/science.1098704.
Meir, T., Orton, P.M., Pullen, J., Holt, T., Thompson, W.T., Arend, M.F., 2013. Forecasting the new York City urban heat island and sea breeze during extreme heat events. Weather Forecast. 28 (6), 1460–1477. https://doi.org/10.1175/WAF-D-13-00012.1.
Middel, A., AlKhaled, S., Schneider, F.A., Hagen, B., Coseo, P., 2021. 50 grades of shade. Bull. Am. Meteorol. Soc. 102 (9), E1805–E1820. https://doi.org/10.1175/BAMS-D-20-0193.1.
Nadolski, V., 1992. Automated Surface Observing System User's Guide. NOAA Publication 12, p. 94.
Nogueira, M., Hurduc, A., Ermida, S., Lima, D.C., Soares, P.M., Johannsen, F., Dutra, E., 2022. Assessment of the Paris urban heat island in ERA5 and offline SURFEX-TEB (v8. 1) simulations using METEOSAT land surface temperature product. Geosci. Model Dev. Discuss. 1–29 https://doi.org/10.5194/gmd-2021-431.
Noh, Y., Cheon, W.G., Hong, S.Y., Raasch, S., 2003. Improvement of the K-profile model for the planetary boundary layer based on large eddy simulation data. Bound.-Layer Meteorol. 107, 401–427. https://doi.org/10.1023/A:1022146015946.
Notaro, M., Holman, K., Zarrin, A., Fluck, E., Vavrus, S., Bennington, V., 2013. Influence of the Laurentian Great Lakes on regional climate. J. Clim. 26 (3), 789–804. https://doi.org/10.1175/JCLI-D-12-00140.1.
Ohashi, Y., Kida, H., 2002. Local circulations developed in the vicinity of both coastal and inland urban areas: a numerical study with a mesoscale atmospheric model. J. Appl. Meteorol. 41 (1), 30–45. https://doi.org/10.1175/1520-0450(2002)041<0030:lcditv>2.0.co;2.
Oke, T., 1982. The energetic basis of the urban heat island, Q. J. Royal Meteorol. Soc. 108 (455) https://doi.org/10.1256/smsqj.45501.
Oke, T., 1995. The heat island of the urban boundary layer: Characteristics, causes and effects. In: Wind Climate in Cities. Springer, Dordrecht, pp. 81–107. https://doi.org/10.1007/978-94-017-3686-2_5.
Prakash, S., Shati, F., Norouzi, H., Blake, R., 2019. Observed differences between near-surface air and skin temperatures using satellite and ground-based data. Theor. Appl. Climatol. 137 (1), 587–600. https://doi.org/10.1007/s00704-018-2623-1.
Qian, Y., Chakraborty, T.C., Li, J., Li, D., He, C., Sarangi, C., Chen, F., Yang, X., Leung, R.L., 2022. Urbanization impact on regional climate and extreme weather: current understanding, uncertainties, and future research directions. Adv. Atmos. Sci. 39, 819–860. https://doi.org/10.1007/s00376-021-1371-9.
Raymond, C., Matthews, T., Horton, R.M., 2020. The emergence of heat and humidity too severe for human tolerance. Sci. Adv. 6(19), eaaw1838 https://doi.org/10.1126/sciadv.aaw1838.
Ribeiro, F.N., de Oliveira, A.P., Soares, J., de Miranda, R.M., Barlage, M., Chen, F., 2018. Effect of sea breeze propagation on the urban boundary layer of the metropolitan region of Sao Paulo, Brazil. Atmos. Res. 214, 174–188.
Rothfusz, L., 1990. The Heat Index (or, More than you Ever Wanted to Know about Heat Index), Technical Attachment SR 90–23. Scientific Services Division, National Weather Service, Fort Worth.
Ryu, Y.H., Smith, J.A., Bou-Zeid, E., Baeck, M.L., 2016. The influence of land surface heterogeneities on heavy convective rainfall in the Baltimore–Washington metropolitan area. Mon. Weather Rev. 144 (2), 553–573. https://doi.org/10.1175/mwr-d-15-0192.1.
Salamanca, F., Krpo, A., Martilli, A., Clappier, A., 2010. A new building energy model coupled with an urban canopy parameterization for urban climate simulations—part I. formulation, verification, and sensitivity analysis of the model. Theor. Appl. Climatol. 99 (3), 331–344. https://doi.org/10.1007/s00704-009-0142-9.
Salamanca, F., Martilli, A., Tewari, M., Chen, F., 2011. A study of the urban boundary layer using different urban parameterizations and high-resolution urban canopy parameters with WRF. J. Appl. Meteorol. Climatol. 50 (5), 1107–1128. https://doi.org/10.1175/2010jamc2538.1.
Sarangi, C., Qian, Y., Li, J., Leung, L.R., Chakraborty, T.C., Liu, Y., 2021. Urbanization amplifies nighttime heat stress on warmer days over the US. Geophys. Res. Lett. 48(24), e2021GL095678 https://doi.org/10.1029/2021gl095678.
Schwab, D.J., Leshkevich, G.A., Muhr, G.C., 1992. Satellite measurements of surface water temperature in the Great Lakes: Great Lakes coast watch. J. Great Lakes Res. 18 (2), 247–258. https://doi.org/10.1016/s0380-1330(92)71292-1.
Sharma, A., Fernando, H.J., Hamlet, A.F., Hellmann, J.J., Barlage, M., Chen, F., 2017. Urban meteorological modeling using WRF: a sensitivity study. Int. J. Climatol. 37 (4), 1885–1900. https://doi.org/10.1002/joc.4819.
Sherwood, S.C., 2018. How important is humidity in heat stress? J. Geophys. Res. Atmos. 123, 11808–11810. https://doi.org/10.1029/2018JD028969.
Skamarock, W.C., Klemp, J.B., 2008. A time-split non- hydrostatic atmospheric model for weather research and forecasting applications. J. Comput. Phys. 227, 3465–3485. https://doi.org/10.1016/j.jcp.2007.01.037.
Smith, T.T., Zaitchik, B.F., Gohlke, J.M., 2013. Heat waves in the United States: definitions, patterns and trends. Clim. Chang. 118 (3), 811–825. https://doi.org/10.1007/s10584-012-0659-2.
Solomon, S., Qin, D., Manning, M., Chen, Z., Marquis, M., Averyt, K.B., Tignor, M., Miller, H.L., 2007. IPCC Fourth Assessment Report (AR4). Climate Change 2007: The Physical Science Basis. Contribution of Working Group I to the Fourth Assessment Report of the Intergovernmental Panel on Climate Change. Cambridge University Press, Cambridge, United Kingdom and New York, NY, USA, p. 996.
Steadman, R.G., 1971. Indices of windchill of clothed persons. J. Appl. Meteorol. 10 (4), 674–683. https://doi.org/10.1175/1520-0450(1971)010<0674:iowocp>2.0.co;2.
Steadman, R.G., 1979. The assessment of sultriness Part I: a temperature-humidity index based on human physiology and clothing science. J. Appl. Meteorol. 18, 861–873. https://doi.org/10.1175/1520-0450(1979)018<0861:TAOSPI>2.0.CO;2.
Stipanuk, G., 1973. Algorithms for Generating a Skew-T, Log P Diagram and Computing Selected Meteorological Quantities. Atmospheric Sciences Laboratory. U.S. Army Electronics Command White Sands Missile Range, New Mexico 88002. https://doi.org/10.21236/ad0769739.
Stull, R., 2011. Wet-bulb temperature from relative humidity and air temperature. J. Appl. Meteorol. Climatol. 50 (11), 2267–2269. https://doi.org/10.1175/jamc-d-11-0143.1.
Sun, L., Liang, X.Z., Xia, M., 2020. Developing the coupled CWRF-FVCOM modeling system to understand and predict atmosphere-watershed interactions over the Great Lakes region. J. Adv. Model. Earth Sys. 12 (12) https://doi.org/10.1029/2020ms002319.
Tan, J., Zheng, Y., Tang, X., Guo, C., Li, L., Song, G., Zhen, X., Yuan, D., Kalkstein, A.J., Li, F., Chen, H., 2009. The urban heat island and its impact on heat waves and human health in Shanghai. Int. J. Biometeorol. 54, 75–84. https://doi.org/10.1007/s00484-009-0256-x.
Thompson, G., Rasmussen, R.M., Manning, K., 2004. Explicit forecasts of winter precipitation using an improved bulk microphysics scheme. Part I: Description and sensitivity analysis. Mon. Weather Rev. 132, 519–542. https://doi.org/10.1175/1520-0493(2004)132<0519:efowpu>2.0.co;2.
Thompson, G., Field, P.R., Rasmussen, R.M., Hall, W., 2008. D.: explicit forecasts of winter precipitation using an improved bulk microphysics scheme. Part II: implementation of a new snow parameterization. Mon. Weather Rev. 136 (12), 5095–5115. https://doi.org/10.1175/2008mwr2387.1.

Umezaki, A.S., Ribeiro, F.N.D., de Oliveira, A.P., Soares, J., de Miranda, R.M., 2020. Numerical characterization of spatial and temporal evolution of summer urban heat island intensity in São Paulo, Brazil. Urban Clim. 32, 100615 https://doi.org/10.1016/j.uclim.2020.100615.

Wang, J., Hu, X.M., 2021. Evaluating the performance of WRF urban schemes and PBL schemes over Dallas–Fort Worth during a dry summer and a wet summer. J. Appl. Meteorol. Climatol. 60 (6), 779–798. https://doi.org/10.1175/JAMC-D-19-0195.1.

Wang, J., Xue, P., Pringle, W., Yang, Z., Qian, Y., 2022. Impacts of lake surface temperature on the summer climate over the Great Lakes region. J. Geophys. Res.-Atmos. 127 https://doi.org/10.1029/2021JD036231.

Xue, P., Pal, J.S., Ye, X., Lenters, J.D., Huang, C., Chu, P.Y., 2017. Improving the simulation of large lakes in regional climate modeling: two-way lake–atmosphere coupling with a 3d hydrodynamic model of the Great Lakes. J. Clim. 30 (5), 1605–1627. https://doi.org/10.1175/jcli-d-16-0225.1.

Yaglou, P., Minard, D., 1957. Control of heat casualties at military training camps. Am. A Arch. Ind. Health 16, 302–316. https://www.cabdirect.org/cabdirect/abstract/19582900896.

Zhao, L., Oleson, K., Bou-Zeid, E., Krayenhoff, E.S., Bray, A., Zhu, Q., Oppenheimer, M., 2021. Global multi-model projections of local urban climates. Nat. Clim. Chang. 11 (2), 152–157. https://doi.org/10.1038/s41558-020-00958-8.

Zobel, Z., Wang, J., Wuebbles, D.J., Kotamarthi, V.R., 2017. High-resolution dynamical downscaling ensemble projections of future extreme temperature distributions for the United States. Earth's Future 5 (12), 1234–1251. https://doi.org/10.1002/2017ef000642.